Cloud Top Liquid Water from Lidar Observations of Marine Stratocumulus

J. D. SPINHIRNE, R. BOERS* AND W. D. HART†

NASA/Goddard Space Flight Center, Laboratory for Atmospheres, Greenbelt, Maryland

(Manuscript received 27 August 1987, in final form 29 February 1988)

ABSTRACT

Marine stratus clouds were simultaneously observed by nadir Nd:YAG lidar measurements and in situ cloud physics measurements. A procedure was applied to derive the two-dimensional vertical cross section of the liquid water from within the cloud top lidar observations. A comparison to direct in-cloud liquid water observations gave good results. The liquid water retrieval was limited to an effective optical depth of 1.5. The true cloud optical thickness was also obtained from the retrieval procedure to a corresponding limit of 3.8. The optical thickness of the observed marine stratus clouds was predominantly below 3.0.

1. Introduction

In this paper, we will describe a study to obtain the liquid water at the tops of marine stratocumulus clouds from lidar observations. Although liquid water may be obtained from in situ measurements, only one-dimensional observations are possible. The advantage of a remote sensing observation from lidar of liquid water within a cloud is that a high resolution, two-dimensional distribution of the liquid water may be realized as opposed to a line measurement from in situ observations. Therefore, a much greater coverage and resolution for the vertical profile of liquid water is possible. Also, the liquid water distribution may be directly related to the convective cloud top height distribution.

The distribution of liquid water at the top of marine stratus clouds is a significant parameter. Marine stratus is important climatologically since the cloud type has a significant global influence on the balance between reflected visible and emitted thermal radiation (Randall 1984). The vertical distribution of liquid water has a direct relation to the radiative and dynamical interactions within the clouds. The formation and structure of marine stratus clouds are maintained largely by radiative cooling at the cloud top (Randall 1980; Schubert et al. 1979), and models have shown that the interaction between radiative cooling and the cloud development are a function of the distribution of the liquid water at the cloud top (Alves 1987).

Lidar observations of marine stratus tops were obtained in 1983 during an experiment off the coast of California which involved the NASA ER-2 aircraft. During the experiment, cloud top lidar observations from the ER-2 were accompanied by simultaneous cloud physics measurement within the cloud. A procedure by which the cloud liquid water may be obtained from lidar observations will be presented. The combined dataset with lidar and in situ measurements will allow us to test the validity of the liquid water retrieval. An analysis of the data case presented here which emphasizes the cloud top boundary structure and its relation to meteorological variables is given in Boers et al. (1988). The extension of these studies will be to relate the liquid water distribution to meteorological parameters and to apply the analysis to observations that have been obtained in subsequent combined field experiments.

2. Calculation procedure

Application of lidar measurements from clouds has been under study for a number of years. Much of the emphasis for lidar cloud studies has been on signal depolarization (e.g., Sassen and Petrillo (1986) have investigated lidar depolarization signals from marine stratus cloud bases) and lidar analysis of cirrus has also been important (Platt 1979). In general, quantitative interpretation of the cloud return signal is complex. The interpretation is simplified when it is recognized that the cloud medium is composed entirely of spherical water drops since single scattering from spherical particles is well known. However, variable droplet size, signal attenuation and multiple scattering must still be considered.

Our retrieval of liquid water from a lidar return signal will have two principal steps. First, the volume scattering cross section is obtained from the lidar return,

* Department of Meteorology, University of Maryland, College Park, Maryland.

† Science Systems Applications, Inc., Lanham, Maryland.

Corresponding author address: Dr. J. D. Spinhirne, Code 617, Lab. for Atmospheres, GSFC, Greenbelt, Maryland 20771.

and second, the volume scattering cross section must be related to the liquid water content. The scattering cross section will be obtained from a solution of the lidar return equation. The liquid water will be derived from the scattering cross section through application of a model based on the available in situ particle measurements.

a. Analysis of lidar data

The lidar return signal is a function of the backscatter from the medium multiplied by two-way path attenuation through the medium. In the case of a cloud signal where the scattering medium is dense, the signal is rapidly dominated by attenuation. The first procedure of the lidar equation solution is a correction for signal attenuation.

The lidar return equation may be written in normalized form as

$$S(Z) = \frac{CB(Z)}{(Z - Z_0)^2} e^{-2\int_{Z_0}^{Z} \sigma(Z')\eta(Z')dZ'}, \quad (1)$$

where $S(Z)$ is the signal in relative units, C a dimensional constant and Z the distance from a receiver located at Z_0. The atmospheric 180° backscatter cross section is given as $B(Z)$ and is the sum of the cloud, aerosol, and molecular backscatter cross sections. The signal attenuation is represented by the term within the exponential where $\sigma(Z)$ is the total extinction cross section. For lidar propagation in a dense medium such as clouds, it is well known that multiple scattering is a significant factor. Cloud droplet scattering at optical wavelengths is highly peaked in the forward direction, and as described by Kunkel and Weinman (1976), Platt (1981) and others, the effect of the multiple scattering is to reduce the apparent attenuation. The factor $\eta(Z)$ is defined, as in Platt (1979), to account for the multiple scattering effect, and the exponential term defines the apparent attenuation. In the analysis to follow, molecular and aerosol scattering at the cloud altitude is assumed to be negligibly small. Also, the aerosol and molecular transmission term above the cloud is assumed constant. Thus, the above cloud transmission may be factored into the dimensional constant C and does not need to be explicitly known.

Calculation of attenuation from equations in the form of (1) for radar and lidar were originally developed for radar rainfall measurements (Hitschfeld and Borden 1954), and there have since been application to lidar data, for example Shipley et al. (1974) and Fernald et al. (1972). Analytic solutions of (1) may be readily derived by which scattering cross sections are obtained from the signal return. For our analysis, the solution of the return equation will be given in terms of the attenuated backscatter cross section $B'(Z)$ where

$$B'(Z) = S(Z)(Z - Z_0)^2/C$$

$$= B(Z)\, e^{-2\int_{Z_0}^{Z} \sigma(Z')\eta(Z')dZ'}. \quad (2)$$

The attenuated backscatter is the fundamental parameter which is obtained from lidar observations.

The solution equation which gives the backscatter cross section from the attenuated backscatter cross section is given as

$$B(Z) = B'(Z) \Big/ \left[1 - \frac{2\eta}{k}\int_{Z_0}^{Z} B'(Z')dZ'\right]. \quad (3)$$

For the derivation of the above equation see for example Platt (1979) or Spinhirne et al. (1980). In the equation as written, the term k which is defined as the ratio of backscatter to extinction cross section, $B(Z)/\sigma(Z)$, and the multiple scattering terms η are considered constant and taken outside the integral term. Constant values for η and k are not strictly correct but are an approximation which is applied in our analysis.

Surprisingly, the assumption of a constant backscatter to extinction ratio is a good approximation for water clouds. Calculations by Pinnick et al. (1983) and related calculations by Derr (1980) show that at visible wavelengths the backscatter to extinction ratio is nearly constant over the range of droplet size distributions which have been measured in water clouds. Pinnick et al. shows that there is a theoretical basis for the result. In addition, calculations of multiple scattering for laser propagation in clouds such as by Kunkel and Weinman (1976) or Platt (1981) indicate that at some depth into the cloud, the η factor tends toward a constant value although the variation can be as much as 50%. The actual optical thickness at which the multiple scatter factor becomes constant and the functional behavior near the cloud boundary is variable and is a function of the cloud scattering phase function, the field of view of the lidar receiver and the distance from the receiver to the cloud boundary. In this study, a constant value for the η factor will be assumed, and the validity of the assumption will be addressed as part of the results from analysis of the experimental data.

Applications of the signal solution Eq. (3) have been widely discussed. The major concern has been that the solution "blows up"' when applied to optically thick media. When the signal is dominated by attenuation, as will be the case at some propagation distance into a dense media, a small error in the effective ratio of extinction to backscatter (η/k as written here) will result in a large error in the cross section solution. However, there are two obvious techniques which overcome the divergent solution problem. The first is to limit the solution to small optical thickness where the attenuation correction will be sufficiently accurate. The second method is to have a boundary condition of a known cross section at a point in the medium to which the solution may be tied. Both of these techniques were involved, for example, in the solution of Fernald et al. (1972) for the retrieval of scattering cross sections from lidar observations of aerosol structure. For our analysis,

the procedure will be to apply the signal solution to only a limited range of cloud depth.

In the case of our lidar observations of marine stratus tops, the optical thickness limit to which the solution may be applied is defined in practice by the nature of the lidar return signal. For the characteristics of the lidar system flown onboard the ER-2, the relatively low transmit power, small aperture, distance to the target and intense background light reflected by the cloud tops give rise to a limited signal-to-noise ratio. As a result, the lower limit of signal detection where the cloud return signal is dominated by noise defines the cloud depth limit for the attenuation correction.

In order to apply (3), the value for η/k, which will be referred to as the effective backscatter to extinction ratio, must be derived. The procedure as developed by Platt (1979) for cirrus clouds is used. If the attenuated backscatter as defined in (2) is integrated to the limit of an infinitely thick media, the result is

$$\int B'(Z) = k/2\eta \quad \text{as} \quad \tau \Longrightarrow \infty. \tag{4}$$

Thus, when the lidar cloud return signal for a sufficiently dense cloud is integrated, the result would be equal to one-half the effective backscatter to extinction factor. In practice, there may be regions of small optical thickness even for stratus clouds, and the maximum value which the integrated signal tends toward for all cloud returns will be used as the appropriate value, as will be described in a following section.

Parenthetically, the behavior of the attenuation correction at the high optical thickness limit of the signal return may be applied to judge the first order validity of the result. A divergent solution, where the denominator of (3) becomes vanishingly small would indicate that the value of η/k was too small. For an optically thick cloud it might also be expected that the scattering cross section would tend toward a constant rather than discontinuous behavior as a function of penetration depth into the cloud. A signal solution may be formulated which would be based on the boundary condition of an assumed homogeneous scattering cross section at large optical depth into the cloud. However, the validity of a constant scattering cross section would not be accurate in most cases, and in addition, the low signal-to-noise ratio for the lidar signal at higher optical depth into the cloud would make the boundary condition solution, as suggested in Klett (1982), unworkable. Therefore, the approach which applies the integrated backscatter values is used, and the behavior of the attenuation correction at the high optical thickness limit is a partial test of the result.

The analysis described above will give a value for the apparent attenuation as a function of cloud depth. For our given assumptions, the effective optical thickness will be

$$\tau'(Z) = -\ln\left(1 - \frac{2\eta}{k}\int_{Z_0}^{Z} (B'(Z')dZ)'\right)\Big/2. \tag{5}$$

However, since the value computed by Pinnick et al. (1983) for k may be applied, the assumed true optical thickness will be obtained from the analysis where

$$\sigma(Z) = B(Z)/k \tag{6}$$

and

$$\tau(Z) = \frac{1}{k}\int_{Z_0}^{Z} B(Z')dZ'. \tag{7}$$

By definition $\eta = \tau'/\tau$, and thus the analysis gives a value for η which may be compared to theoretical estimates.

b. Liquid water calculation

To a first approximation, the ratio between liquid water content W and the cloud extinction coefficient is given by (Twomey 1977):

$$W/\sigma = \frac{2}{3}\rho\langle r\rangle \tag{8}$$

where $\langle r\rangle$ is the mode radius and ρ is the density of water. Then

$$W(Z) = \frac{2B(Z)\rho}{3k}\langle r(Z)\rangle. \tag{9}$$

A more accurate calculation which accounts for size distribution variability may be obtained from use of the expression in Pinnick et al. (1983):

$$W = \frac{2\rho B}{3k}\left[\frac{\langle r^3\rangle}{\langle r^2\rangle} - \delta\omega^2\frac{\langle r^4\rangle\langle r^3\rangle}{\langle r^2\rangle\langle r^2\rangle} + O(\delta^2)\right] \tag{10}$$

where ω is the wavenumber and k and δ are curve-fit parameters derived by Pinnick et al. When extrapolated to the 0.532 μm doubled Nd:YAG laser wavelength the values are $1/k = 17.6$ and $\delta = 2.2 \times 10^{-6}$. In order to calculate $W(Z)$ from the lidar derived $B(Z)$, a model for the particle size distribution based on in-cloud measurements will be applied.

3. Experimental

a. Lidar observations

The cloud and aerosol lidar system on the ER-2 aircraft is a compact, automated, Nd:YAG laser-based instrument which was designed to operate from high altitude aircraft and to observe elastic backscatter from the atmosphere in the nadir direction. Prior to 1983, the system had flown onboard a WB-57F aircraft and had been described previously by Spinhirne et al. (1983). However, the system was transferred to the ER-2 aircraft in 1983, and improvements were also made to the signal acquisition capabilities of the instrument. The return signal at the 1.064 μm fundamental laser wavelength is currently detected along with

the dual polarization detection of the 0.532 μm doubled wavelength. In addition, the sensitivity, stability and dynamic range of the signal detection were improved so that the entire range of atmospheric scattering, from molecular and aerosol scattering to scattering from the most dense clouds, can be retrieved from the data with appropriate signal processing. A list of system characteristics is given in Table 1. The signals are, by necessity, compressed with four decade logarithmic amplifiers. A critical aspect of the instrument performance was the calibration and dynamic response of the logarithmic amplifiers. The calibration and response were doubly tested by laboratory and field procedures.

The lidar system parameters which are of particular concern for the stratocumulus top observations are the signal acquisition bandwidth, the noise equivalent signal and the system backscatter cross section calibration. The signal acquisition bandwidth is significant for the rise time of the observed scattering. The length of the instantaneous scattering volume of the lidar signal would be 0.6 m for the nominal 8 ns pulse length of the system laser. If 0.6 m or 4 ns is considered the maximum signal rise time, the equivalent system bandwidth would be 87.5 MHz. Since the actual system bandwidth is 10 MHz, giving a 5.25 m equivalent signal range rise time, cloud scattering discontinuities of less than the 7.5 m range sampling interval will not be resolved even by averaging from multiple shot returns.

The noise equivalent signal limits the penetration depth into the cloud for which a backscatter return signal may be used. For daytime observations, the signal noise is almost entirely due to quantum noise induced by the ambient reflected brightness from the sunlit cloud tops. An example of the return signal from a stratocumulus cloud top for a single laser pulse at the full system bandwidth is shown in Fig. 1. In this case, the noise equivalent signal, in terms of attenuated backscatter cross section, is approximately 0.05 (1/km-sr). Since a typical backscatter cross section for stratus is found to be 1.0 (1/km-sr), it follows that the effective optical thickness for which the signal is reduced to the noise level is approximately 1.5.

A calibration of the lidar return signal in terms of backscatter is needed in order to relate the stratocumulus return signal to the attenuated backscatter cross section. The backscatter calibration is obtained from

TABLE 1. Lidar system characteristics.

Laser	Nd:YAG I, II
Wavelength	1.064, 0.532 μm
Pulse energy	65, 35 m J
Pulse rate	3.47–5 Hz
Telescope diam.	17 cm
FOV	1.4 mrad
Filter width	1 nm
Signal channels	P&S polarization
Digitizer	8-bit, 20 MHz
Compression amp.	4 decade logarithmic

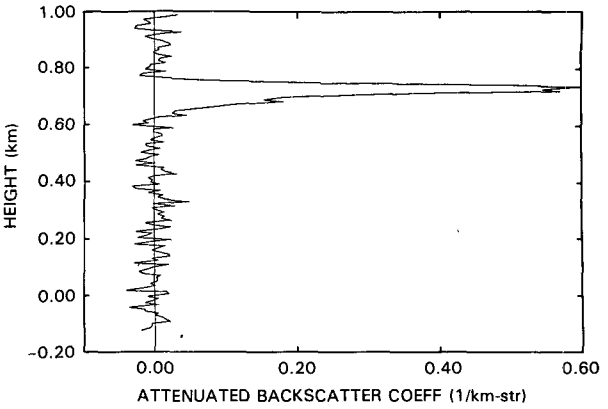

FIG. 1. Single lidar return signal from marine stratus cloud top. The noise equivalent value of the backscatter coefficient is indicated by the fluctuations above and below the cloud signal.

the signal which is received from the upper troposphere and lower stratosphere. The upper atmospheric return is ratioed to the calculated molecular scattering cross section of the atmosphere; at the level of the minimum ratio, aerosol scattering is assumed to be negligible. In 1983, the stratospheric signal from directly under the aircraft was strongly influenced by the El Chichon aerosol layer, but adequate scattering minimums were found in the upper troposphere.

b. Field experiment

An aircraft field experiment to study marine stratus clouds by combined remote sensing and in situ observations was performed in September 1983. The in situ observations were acquired by a Super King Air aircraft as described by Cooper (1983). The in situ measurements of primary concern in this study were liquid water content by a Johnson–Williams probe (see for example Strapp and Schemenauer 1982) and cloud droplet size spectra by a PMS FSSP probe.

The data to be reported in this study were acquired between 20:00 and 22:30 UTC 28 September in a region of the Pacific Ocean approximately 200 km to the southwest of San Francisco. Cirrus interference prevented the analysis of other stratus data cases from the 1983 mission. On 28 September, the two aircraft flew an east–west racetrack pattern with the northern flight line at 20 km to the north of the southern line. The ER-2 was at a constant altitude of approximately 18 km and flew east–west flight legs of approximately 60 km in length. The King Air flew at alternating levels within or near the stratus clouds. The flight patterns were synchronized so that the ER-2 overflew the King Air on the east–west lines. At the time of the flights on 28 September, the experimental area was covered by solid to partially broken stratus clouds. Cloud top heights for the stratus within the experimental area varied from approximately 650 m in the east to 900

m in the west. The meteorology was characterized by moderately high wind shear at the cloud top and a prominent cellular structure within the cloud layer. For a more complete description of the weather conditions and cloud structure during the field experiment see Boers et al. (1988).

4. Results

The lidar return signal from an 8 km flight line segment is plotted in Fig. 2 as a contoured cross section. The flight segment is typical of the data. A signal is obtained from approximately 200 m through the cloud. From the data, the cellular cloud structure is clearly evident, and at one location there is a gap in the cloud deck.

In order to obtain the liquid water content, the lidar data, such as in Fig. 2, is first corrected for attenuation. As was described in section 2, the initial procedure for the attenuation correction of the lidar data is to derive the value of the effective backscatter to extinction ratio from the integrated signal. In practice, a distribution of values for the integrated signal return is found. The distribution arises from both the variability of optical thickness and from signal noise.

In order to identify the true limiting maxima for the integrated backscatter, the integrated backscatter was plotted versus a measure of cloud optical thickness, as shown in Fig. 3. The relative measure of cloud optical thickness which was applied was the visible cloud reflectance. The reflectance is defined as

$$R = \frac{\pi I(\theta_0, \theta, \phi)}{F \cos\theta_0}, \qquad (11)$$

where $I(\theta_0, \theta, \phi)$ is the measured radiance in the downward observation angle θ (in this case nadir) and azimuth angle ϕ relative to the solar plane; θ_0 is the solar zenith angle and F is the normally incident solar irradiance. The radiance measurement was obtained from a multispectral scanning radiometer (Curran et al. 1981) at a narrowband wavelength of 0.75 μm. The radiometer had been optically aligned with the lidar system such that the nadir radiance measurement was directly co-aligned with the laser beam direction. As shown by calculations of stratus cloud reflectance (see,

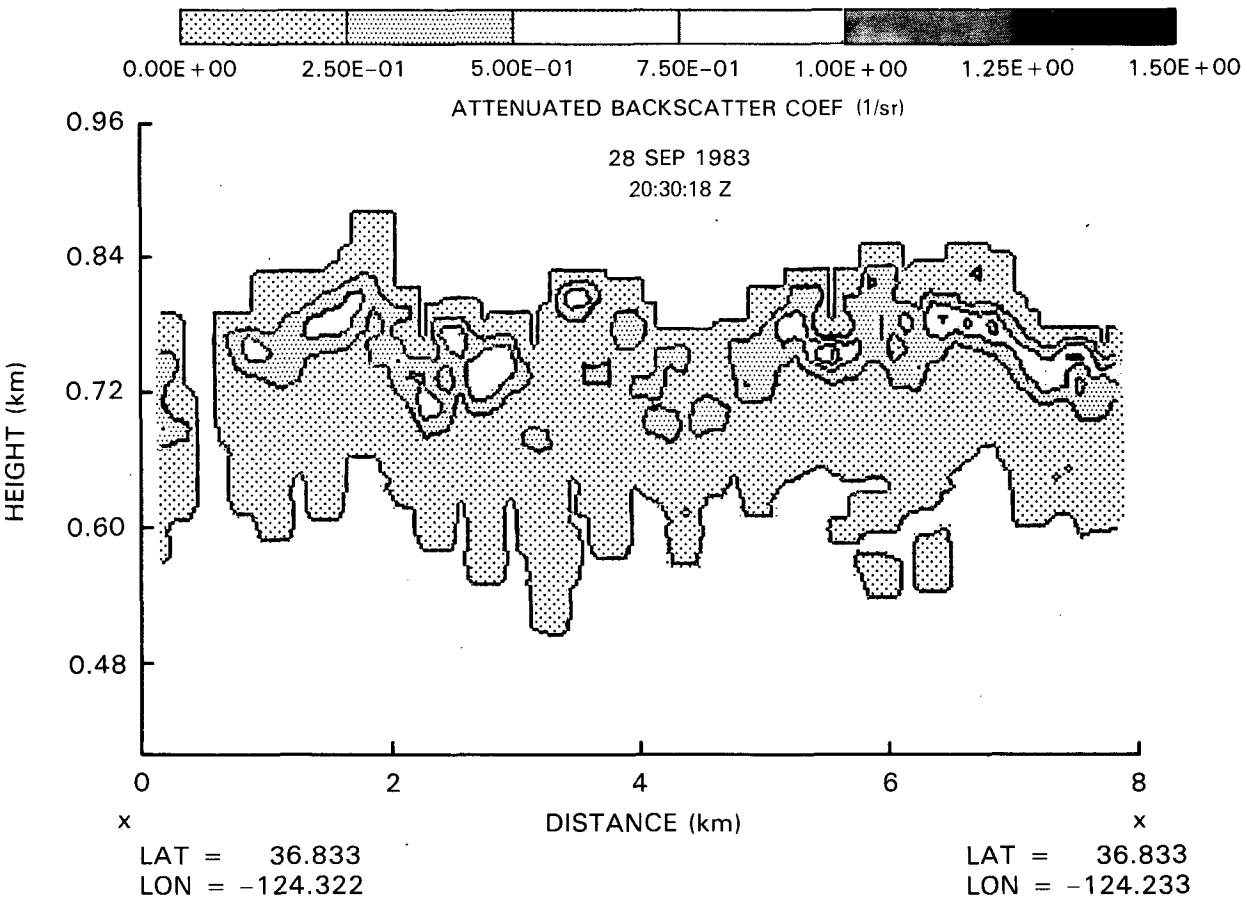

FIG. 2. Contour plot of the received lidar signal from a partial segment of an experiment flight line. The return signal is shown as the attenuated backscatter cross sections.

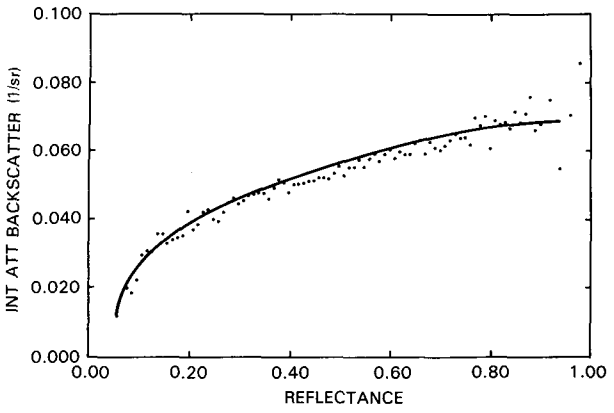

FIG. 3. The vertically integrated attenuated backscatter lidar signal as a function of the cloud top reflectance. The reflectance was obtained from scanning radiometer observations in the nadir direction at a clear wavelength of 0.75 μm. The data points are averages over 0.01 reflectivity increments. The solid line represents a mean fit to the range of values.

for example, King 1987), the reflectance is roughly a linear function of the optical thickness if the optical thickness is less than approximately 10. Model calculations indicate the lidar integrated backscatter tends to saturate at optical thickness approaching three. As in Fig. 3, the distribution of integrated backscatter versus reflectance may be extrapolated to obtain the mean and estimated error of maximum integrated backscatter. The scatter of values in Fig. 3 would result primarily from slope effects of the cloud reflectance such as shadowing. The smooth curve was derived by averaging points into equal intervals of reflectance and empirically fitting to the average values. The value of k/η that was derived for the 28 September observation was 0.14 with an estimated uncertainty of ± 0.01. From Pinnick et al. (1983), $k = 0.057$ which leads to an effective value of 0.41 for the multiple scattering factor η. Theoretical calculations relating to values of η are given by Kunkel and Weinman (1976). As discussed by Spinhirne (1982) multiple scattering is to first order a function of the product of the receiver field of view (FOV) and the range to the cloud boundary. Our case of a 1.4 mr FOV and an approximately 18 km distance from the cloud top would correspond very roughly to KW's calculation for a cumulus cloud at 1 km and a 20 mr FOV. The related multiple scatter factor from KW in that case was 0.55 ± 0.05 which is on the order of the measured value.

As was previously discussed, the droplet size distribution must be known in order to relate the scattering cross section to the liquid water content. The droplet size distribution is a function of the height within the cloud and was obtained from the in situ data. An obvious complication is that the height dependence of the droplet size distribution is a function of horizontal location. The size distribution height dependence would be expected to be different between the center and edges of cloud cells. However, the in situ data can provide only an average height dependence for the size distribution. In order to arrive at size distribution parameters for the liquid water calculation therefore, the in situ data from the entire flight experiment were averaged. The results for the size distribution parameters from the average spectra are given in Fig. 4. The height dependence of the first moment and the ratio of the second and third moments which are applied in (9) are shown. The difference between $\langle r \rangle$ and $\langle r^3 \rangle / \langle r^2 \rangle$ was a function of the skewed shape of the size spectra. A general linear increase of the size parameters with height is evident. For the liquid water calculations, a continuous linear model of the droplet size parameters, indicated in Fig. 3, was applied.

In order to validate the liquid water retrievals based on the lidar data, the cross-sectional profiles of liquid water were calculated along flight lines and compared to the direct in situ measurements by the Johnson–Williams (JW) probe. The liquid water result along one flight line is presented in Fig. 5 for both the lidar and JW measurement. The altitude profile for the in situ measurement is indicated. The direct one-to-one comparison between the lidar and in situ result is problematical from the standpoint of aircraft navigation accuracy. The positional uncertainty of the aircraft inertial navigation systems was on the order of 1 kilometer. In addition, there would be an estimated 60 m uncertainty in the relative height of the two observations. From the figures it may be seen that large changes in cloud density over a 1 km distance is possible. Also, the observation times between the two systems would be different except at the cross point for the two aircraft. However, in Fig. 5, some correlation between the in situ and lidar-derived result is seen. The

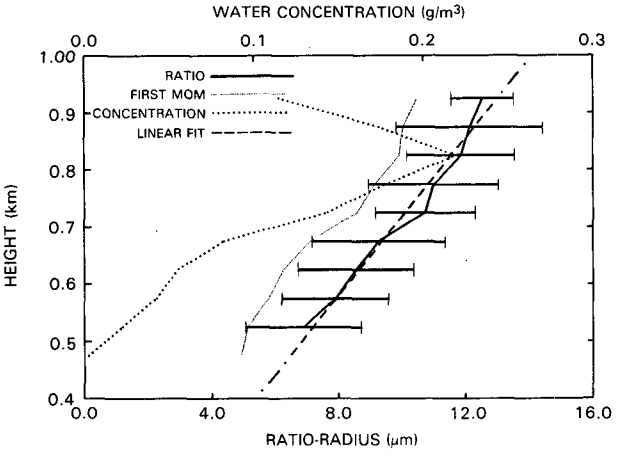

FIG. 4. Results from average of all in situ particle measurements. The average for the first moment and the ratio for the second and third moments of particle radius for the size distribution are shown. The error bars on the ratio represent twice the variance of the observations. The linear fit to the ratio parameter was applied for the lidar calculations.

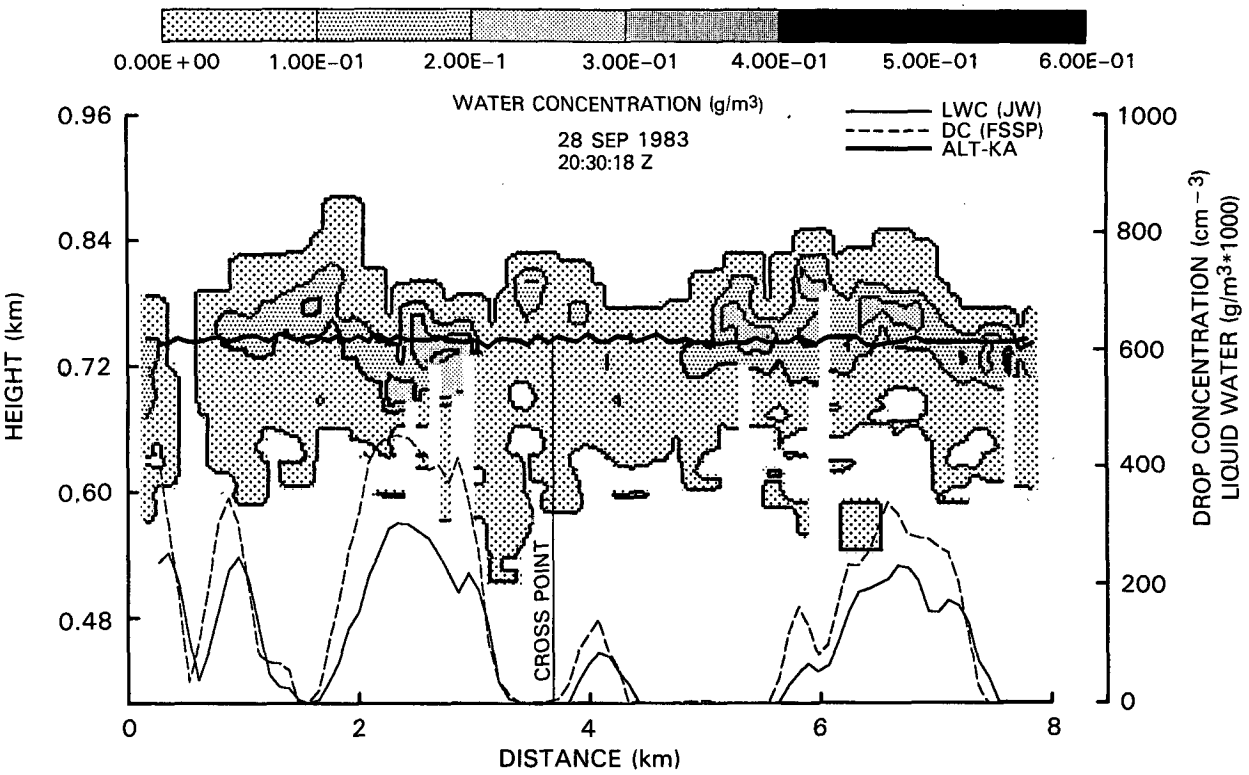

FIG. 5. Calculated liquid water along an eight kilometer segment of one flight line. In addition to the lidar-derived water concentration cross section, the King Air flight line altitude (ALT-KA) through the cloud for near simultaneous in situ observations is indicated. The droplet concentration measured from a PMS FSSP instrument [DC (FSSP)] and liquid water concentration from a Johnson–Williams instrument [LWC (JW)] for the in situ measurement are shown. Some lack of agreement between the lidar and in situ observation would be expected from navigational uncertainties.

location of increased liquid water within convective cells generally agrees, although in some areas, one sensor indicates zero whereas the other is still within the cloud. Liquid water values very near zero are within the lowest shaded region of the lidar-derived value.

The cloud depth limit of the lidar liquid water retrieval is indicated in Fig. 5 in two ways. If the calculated liquid water decreases to the value of the lowest contour limit, a lower contour cloud boundary is shown. If the attenuation limit for the signal solution of 1.5 effective optical thickness is reached, the liquid water calculation is terminated before the lower contour boundary. The latter case in Fig. 5 is indicated by an absence of a lower contour boundary. As shown, in most areas, the cloud layer was sufficiently thin to reach the lower boundary limit.

As given in (7), the optical thickness of the cloud layer may be computed within the effective limit of the solution. The computed optical thickness for the flight line of Fig. 5 is shown in Fig. 6. In regions other than at the center of cloud cells, the optical thickness is seen to be less than 3.0.

As discussed, a comparison of the lidar and in situ liquid water measurements is difficult due to navigation uncertainty and sampling differences. A direct point-to-point comparison is not valid. However, a comparison of average values along the flight track of the in situ aircraft was made. The comparison was possible only on flight legs for which the altitude of the in situ aircraft was within the lidar observed level of the stratus cloud and where there was a close crossover in aircraft

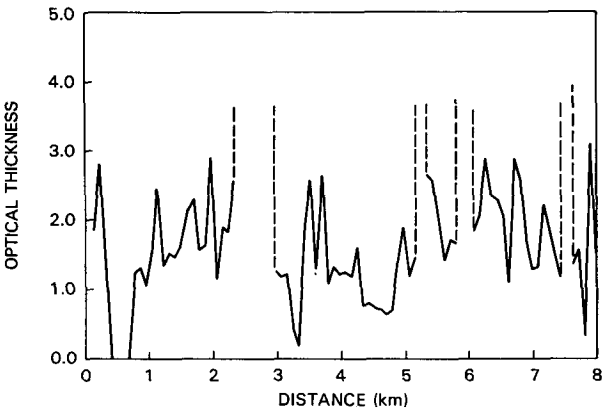

FIG. 6. Calculated optical thickness for the cloud segment which was shown in Fig. 2 and Fig. 5. Areas between dashed lines were beyond the effective solution range.

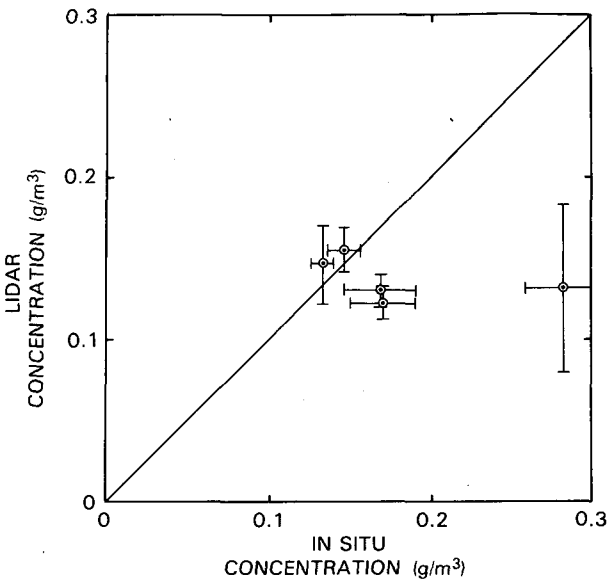

FIG. 7. Comparison between flight line averages for the lidar and in situ values of liquid water concentration. The error bars represent the variances of the measurements.

location. There were five such flight legs during the 28 September experiment, and the values for both the JW and lidar liquid water averaged along the in situ flight tracks are shown in Fig. 7. The agreement of the average values was found to be within the variance of the observations as indicated by the plotted error bars for two of the flight lines and two other values are quite close. On the fifth line, the average for the lidar retrieval is approximately one-half the in situ average. The fifth flight line segment is shown in Fig. 8 and involves a more inhomogeneous cloud layer than for the other flight lines. Because of the inhomogeneity, the variance of the observation is much larger. Either the estimated 60 m uncertainty of the height of the two measurements or the uncertainty of the aircraft navigation could account for the lack of agreement. The direct comparison of observations from an in-cloud aircraft and remote sensing observations from an overflying aircraft is difficult for the reasons given above. However, our results indicate a reasonable validity for the procedure. Direct in-cloud measurement of liquid water is also subject to limitations (Knollenberg 1972).

The uncertainty of the lidar liquid water retrieval will be a function of the variability of the size distribution parameter. The variability is indicated in Fig. 4 and is approximately 20%. There could, however, be a systematic bias in that smaller droplet sizes would most likely be associated with the less dense cloud areas between cells, and in that case, the liquid water would be underestimated. However, the net bias would have the effect to increase the variance of the derived liquid

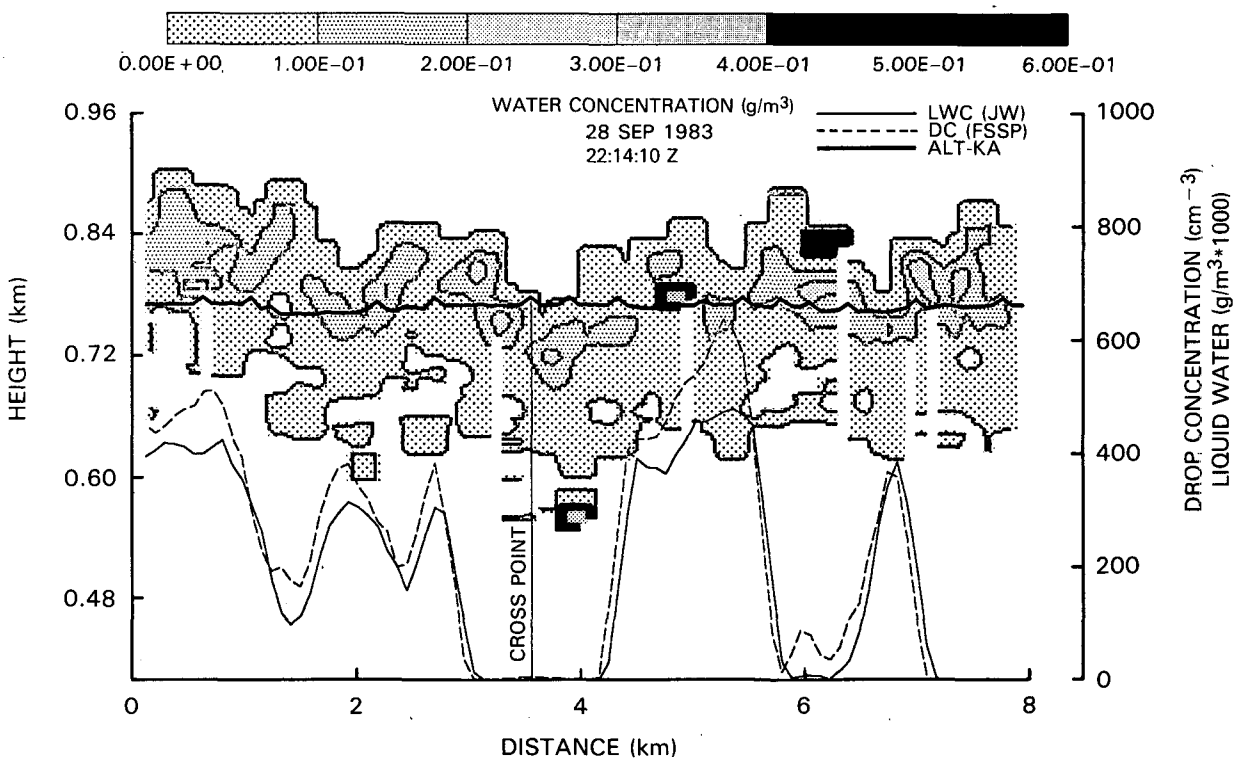

FIG. 8. As in Fig. 5 but for an alternate time. The cloud structure for the line is more inhomogeneous and the comparison between the remote and direct observations is thus more uncertain.

water. As may be seen in Fig. 7, the variance of the lidar observation is not significantly larger on average than the in-cloud measurement.

Another possible bias of the observation is the derived constant value for k/η. In practice, the effect of signal noise will lead to an uncertainty in the maximum value of the integrated backscatter signal for the lidar return data. The noise-induced error may lead to errors in the attenuation corrections. The integral result of (4) assumes, as was previously described, that the effective backscatter to extinction factor is constant. When the integral derived value of k/η is applied to the attenuation correction of the lidar return signal, an error may result due to the fact that the true behavior of the effective backscatter to extinction ratio is not absolutely constant. Further modeling studies may be needed to adequately judge the effect, but no large influence is evident in our results.

An additional comparison between the lidar-retrieved liquid water and directly measured values is shown in Fig. 9. The data is from a single 44 km flight line where the in situ aircraft had flown at different altitudes along the track. The average vertical profile from the direct measurement is shown. Also given is the water concentration profile derived from lidar data values along a 30 m altitude band for the track followed by the in situ aircraft. The profiles are in agreement, although deviations due to the limited sampling are evident. The lack of lidar values above 0.8 km along track would be due to navigation and time differences between the aircraft as discussed previously. The additional profile in Fig. 9 is the average for all lidar values for the cloud cross section along the flight track. The larger data sample produces a much smoother average for water concentration profile and significant additional detail, including the decrease in concentration at the cloud top, as shown. The lidar retrieval can thus present a much more representative vertical profile from sampling over a limited cloud area.

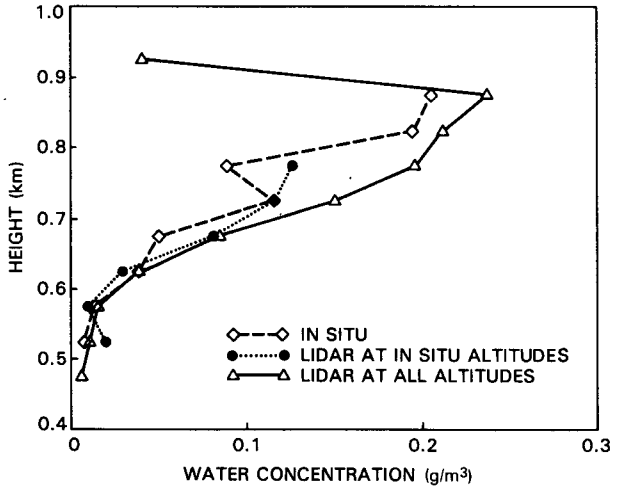

FIG. 9. Comparison between the vertical profile of the average liquid water concentration derived from the in situ and lidar measurements. The results are from a single 44 km flight line. The lidar result is shown both for all the data along the cloud cross section and for only data points which are along the altitude track of the in situ aircraft.

The requirement for knowledge of the droplet size distribution parameters is the primary limitation for the visible wavelength lidar retrievals of cloud liquid water. As discussed by Platt and Takoshima (1987), the ratio between extinction and cloud liquid water is independent of droplet size for lidar measurements at CO_2 laser wavelengths (9–10 μm region), and thus a procedure such as was applied here for visible lidar measurements could possibly be more directly applied for CO_2 lidar measurements. However, at the CO_2 laser wavelengths, the ratio of extinction to backscatter cross section is not independent of droplet size as for the visible lidar (Pinnick et al. 1983). Thus, since droplet size varies with location in typical clouds, the attenuation correction for a CO_2 lidar measurement may require a knowledge of the droplet size parameters. A multiwavelength approach could be studied, and it has been suggested that lidar signal depolarization (Carswell and Pal 1980) or passive radiance analysis (Curran et al. 1981) could be applied as a measure of droplet size. However, even without more advanced observation techniques, our results indicate that in a combined experiment involving remote and in-cloud measurements, the lidar observations are a useful adjunct measurement for describing the spatial variability of cloud liquid water.

5. Conclusion

Lidar observations of cloud tops provide data on the vertical and horizontal cloud structure that is not possible with in situ measurements. A procedure was described by which the lidar data can be related to the cloud top liquid water content. The lidar liquid water observations are limited to an effective cloud optical depth of approximately 1.5. In general, good agreement in the average values of liquid water was found between lidar-derived values and values obtained from direct observations by a Johnson–Williams probe. The agreement was obtained even though there are many difficulties associated with a direct comparison of in-cloud and remotely sensed results.

The lidar-cloud liquid water calculation required a size distribution mode radius parameter, and a model derived from in situ droplet measurements was applied. The uncertainty for the mode radius parameter is the primary error source of the liquid water retrieval from the visible wavelength lidar data. However, our study indicates that the lidar result provides a useful supplement to direct in-cloud observations. Independent visible wavelength lidar measurements of cloud top liquid water distribution could be derived if an appropriate model or alternate remote sensing technique for the mode radius parameter were available.

The liquid water retrieval was attempted for a single marine stratus cloud case. The cloud layer exhibited a pronounced cellular structure. From the analysis procedure the cloud optical thickness was also derived. The cloud thickness was such that in most areas liquid water was retrieved through the base of the layer, and the total optical thickness was thus less than 3.0. A complete description of the meteorology for the cloud case and other associated measurements is given in Boers et al. (1988) and Boers and Betts (1988). A more general situation for marine stratus would likely have greater homogeneity and optical thickness than the case which was studied here. The liquid water retrieval should produce more accurate results for clouds of greater homogeneity.

The current application for the lidar observation of cloud liquid water is as an enhancement to the interpretation of data obtained during a marine stratus field experiment. Although the basic lidar signal will reveal the convective cloud structure and height, the structure is more meaningful when converted to liquid water parameters. For small-scale variations, greater resolution of the vertical distribution of liquid water can thus be obtained than by direct measurements. A much greater database of marine stratus observations by combined remote and direct observations has now been obtained through the 1987 First International Satellite Cloud Climatology Progam (ISCCP) Regional Experiment (FIRE). Analysis of lidar cloud observations as described in this paper will likely play a role in studies with the FIRE dataset.

Acknowledgments. The authors would like to thank Joanne Simpson for her support in organizing and carrying out the marine stratus observation experiment. This work was supported by the NASA Mesoscale Meteorology and Climate Research Programs.

REFERENCES

Alves, A. R., 1987: Interaction of longwave radiation, microphysics and turbulence in boundary layer clouds. Ph.D. dissertation, Purdue University.

Boers, R., and A. K. Betts, 1988: Saturation point structure of marine stratocumulus clouds. *J. Atmos. Sci.*, **45,** 1156–1175.

——, J. D. Spinhirne and W. D. Hart, 1988: Lidar observations of the fine-scale variability of marine stratocumulus clouds. (accepted for publication in *J. Climate Appl. Meteor,* **27,** 797–810.

Carswell, A. I., and R. S. Pal, 1980: Polarization anistropy in lidar multiple scattering from clouds. *Appl. Opt.*, **19,** 4123–4126.

Cooper, W. A., 1978: Cloud physics investigations by the University of Wyoming in HIPLEX, 1977. University of Wyoming report 119.

Curran, R. J., H. L. Kyle, L. R. Blaine, J. Smith and T. D. Clem, 1981: Multichannel scanning radiometer for remote sensing cloud physical parameters. *Rev. Sci. Instrum.*, **52,** 1546–1555.

Derr, V. E., 1980: Estimation of the extinction coefficient of clouds from multiwavelength lidar backscatter measurements. *Appl. Opt.*, **19,** 2310–2314.

Fernald, F. G., B. M. Herman and J. A. Regan, 1972: Determination of aerosol height distributions by lidar. *J. Appl. Meteor.*, **11,** 482–499.

Hitschfeld, W., and J. Bordan, 1954: Errors inherent in the radar measurement of rainfall at attenuating wavelengths. *J. Meteor.*, **11,** 58–67.

King, M. D., 1987: Determination of the sealed optical thickness of clouds from reflected solar radiation measurements. *J. Atmos. Sci.*, **44,** 1734–1751.

Klett, L. D., 1981: Stable analytical inversion solution for processing lidar returns. *Appl. Opt.*, **20,** 211–220.

Knollenberg, R. G., 1972: Comparative liquid water content measurements of conventional instruments with an optical array spectrometer. *J. Appl. Meteor.*, **11,** 501–508.

Kunkel, K. E., and J. A. Weinman, 1976: Monte Carlo analysis of multiple scattering on light pulses reflected by turbid atmospheres. *J. Atmos. Sci.*, **33,** 1763–1771.

Pinnick, R. G., S. G. Jennings, P. Chylek, C. Ham and W. T. Grandy, 1983: Backscatter and extinction in water clouds. *J. Geophys. Res.*, **88,** 6787–6796.

Platt, C. M. R., 1979: Remote sounding of high cloud. Part I: Calculations of the visible and infrared optical properties from lidar and radiometer measurements. *J. Appl. Meteor.*, **18,** 1130–1143.

——, 1981: Remote sounding of high clouds. Part III: Monte Carlo calculations of multiple-scattered lidar returns. *J. Atmos. Sci.*, **38,** 156–167.

——, and T. Takashima, 1987: Retrieval of water cloud properties from carbon dioxide lidar sounding. *Appl Opt.*, **26,** 1257–1263.

Randall, D. A., 1980: Conditional instability of the first kind upside down. *J. Atmos. Sci.*, **37,** 125–130.

——, 1984: Outlook for research on subtropical marine stratiform clouds. *Bull. Amer. Meteor. Soc.*, **65,** 1290–1301.

Sassen, K., and R. L. Petrillo, 1986: Lidar depolarization from multiple scattering in marine stratus clouds. *Appl. Opt.*, **25,** 1450–1458.

Schipley, S. T., E. W. Eloranta and J. A. Winman, 1974: Measurement of rainfall rates by lidar. *J. Appl. Meteor.*, **13,** 800–807.

Schubert, W. H., J. S. Wakefield, F. Y. Steiner and S. K. Cox, 1979: Marine stratocumulus convection, Part I. *J. Atmos. Sci.*, **36,** 1286–1307.

Spinhirne, J. D., 1982: Lidar clear atmosphere multiple scattering dependence on receiver range. *Appl. Opt.*, **21,** 2467–2468.

——, J. A. Reagan and B. M. Herman, 1980: Vertical distribution of aerosol extinction cross section and inference of aerosol imaginary index in the troposphere by lidar technique. *J. Appl. Meteor.*, **19,** 426–438.

——, M. Z. Hansen and J. Simpson, 1983: The structure and phase of cloud tops as observed by polarization lidar. *J. Climate Appl. Meteor.*, **22,** 1319–1331.

Strapp, J. W., and R. S. Schemenauer, 1982: Calibrations of Johnson–Williams liquid water content meters in a high speed icing tunnel. *J. Appl. Meteor.*, **21,** 98–108.

Twomey, S., 1977: The influence of pollution on the shortwave albedo of clouds. *J. Atmos. Sci.*, **34,** 1149–1152.